Coupled Systems Mechanics, *Vol. 13, No. 4 (2024) 311-335*
https://doi.org/10.12989/csm.2024.13.4.311

Minimum cost design for circular isolated footings with eccentric column taking into account that the surface in contact with the ground works partially in compression

Inocencio Luévanos-Soto[1a], Arnulfo Luévanos-Rojas*[2],
Victor Manuel Moreno-Landeros[2b] and Griselda Santiago-Hurtado[3c]

[1]Facultad de Ingeniería, Ciencias y Arquitectura, Universidad Juárez del Estado de Durango, Av. Universidad S/N, Fracc. Filadelfia, CP 35010, Gómez Palacio, Durango, México
[2]Instituto de Investigaciones Multidisciplinaria, Universidad Autónoma de Coahuila, Blvd. Revolución No, 151 Ote, CP 27000, Torreón, Coahuila, México
[3]Facultad de Ingeniería Civil, Universidad Autónoma de Coahuila, CP 27276, Torreón, Coahuila, México

(Received May 18, 2024, Revised June 30, 2024, Accepted July 1, 2024)

Abstract. This work aims to show a model to estimate the minimum cost (Thickness and area of steel in X and Y directions) for design a circular isolated footing with eccentric column that considers that the surface in contact with the ground works partially under compression. The formulation is shown by integration to find the moments, the bending shears and the punching shear using the pressure volume under the footing. Some researchers show the minimum cost design for circular isolated footings for an eccentric column assuming that the contact area works completely in compression, others consider the contact surface with the ground working partially in compression for a column in the center of the base. Three numerical examples are developed to obtain the complete design, which are: Example 1 for a column in the center of the base, Example 2 for a column at a distance of 1.50 m from the center of the base in the X direction, Example 3 for a column at a distance of 1.50 m from the center of the base in both directions. Also, a comparison of the new model against the model proposed by other authors is presented. The comparison shows that the new model generates a great saving of up to 43.74% for minimum area and 48.44% for minimum cost design in a column located in the center of the base, and when the column is located at a distance of radius/2 starting from the center of the base in the X direction generates great savings of up to 45.24% for minimum area and 31.80% for minimum cost design. Therefore, it is advisable to use the model presented in this study.

Keywords: bending shears; circular isolated footings; minimum cost design; moments; punching shear; surface in contact with the ground works partially under compression

1. Introduction

*Corresponding author, Ph.D., E-mail: arnulfol_2007@hotmail.com
[a]Ph.D. Candidate, E-mail: inocencio.luevanos@ujed.mx
[b]Ph.D., E-mail: victor_moreno_landeros@uadec.edu.mx
[c]Ph.D., E-mail: santiagog@uadec.edu.mx

http://www.techno-press.org/?journal=csm&subpage=8 ISSN: 2234-2184 (Print), 2234-2192 (Online)

A foundation is the support base of the entire structure through which loads are transmitted to the underlying soil. Every foundation must permanently guarantee the stability of the construction it supports.

The main contributions on the bearing capacity of the soil, soil-structure interaction, experimental tests for footings and settlement behavior in foundations under biaxial bending have been presented by several researchers (Ramu and Madhav 2010, Lee *et al.* 2015, Kaur and Kumar 2016, Dagdeviren 2016, Hadzalic *et al*. 2018a, b, c, 2020, Turedi *et al.* 2019, Golewski 2019, Luat *et al*. 2020, Ibrahimbegovic *et al.* 2021).

The most relevant references that address the topic of foundation design, mathematical models for the design and contact surface with the ground for all types of foundations have been presented in the work proposed by Luévanos-Soto *et al*. (2024) (Agrawal and Hora 2012, Aguilera-Mancilla *et al.* 2019, Al-Ansari 2013, 2014, Alijani and Bidgoli 2018, Alazwari *et al.* 2021, Anil *et al.* 2017, Basudhar *et al*. 2012, Garay-Gallegos *et al*. 2022, García-Galván *et al.* 2022a, b, Garcia-Graciano *et al*. 2022Gör 2022, Himeur *et al*. 2022, Jelusic and Zlender 2018, Khajehzadeh *et al*. 2014, Kim-Sanchez *et al*. 2022, Lezgy-Nazargah *et al*. 2022, López-Chavarría *et al*. 2017a, b, c, 2019, Luévanos-Rojas 2014a, b, c, 2015a, b, 2016a, b, c, 2023a, b, c, Luévanos-Rojas *et al.* 2013, 2017a, b, 2018a, b, 2020, 2022, 2024a, Malapur *et al*, 2018, Mohebkhah 2017, Montes-Páramo *et al*. 2023, Moreno-Hernández *et al*. 2022, Pasillas-Orona *et al*. 2020, Rad 2012, Rawat and Mittal 2018, Rivera-Mendoza *et al.* 2022, Rizwan *et al*. 2012, Soto-García *et al*. 2022, Vela-Moreno *et al.* 2022, Velázquez-Santillán *et al*. 2018, Yáñez-Palafox *et al*. 2019).

The current studies closest to the topic of isolated footings are: The minimum cost design assuming that the contact zone with the ground works partially in compression for circular footings proposed by Kim-Sánchez *et al*. (2022) and for rectangular footings investigated by Luévanos-Rojas (2023c), but in these works the column is in the center of the base. The minimum cost design with an eccentric column for rectangular footings (Luévanos-Rojas 2023a) and for circular footings (Luévanos-Rojas *et al*. 2024b), but in these works present the contact zone with the ground working completely under compression.

This study shows a model to estimate the minimum cost design (Thickness and areas of steel in X and Y directions) for circular isolated footings with an eccentric column taking into account that the contact area with the ground works partially in compression, that is, a part of the contact area of the footing is under compression and the other under zero pressure. The formulation is presented by integration to find the factored moments, the factored bending shears and the factored punching shear using the pressure volume under the footing in function of the factored available allowable soil pressure, the radius of the circular footing, the angle of inclination with respect to the Y axis where the resultant moment appears, the location coordinates of the column, the distance from the center of the base to the neutral axis measured on the axis where the resultant moment appears, the sides of the column. Three numerical problems are given to estimate the minimum cost design for circular isolated footings under biaxial bending. In addition, a comparison is made between the new model and the model proposed by other authors to observe the differences.

2. Methodology

2.1 Case I: Area works completely under compression

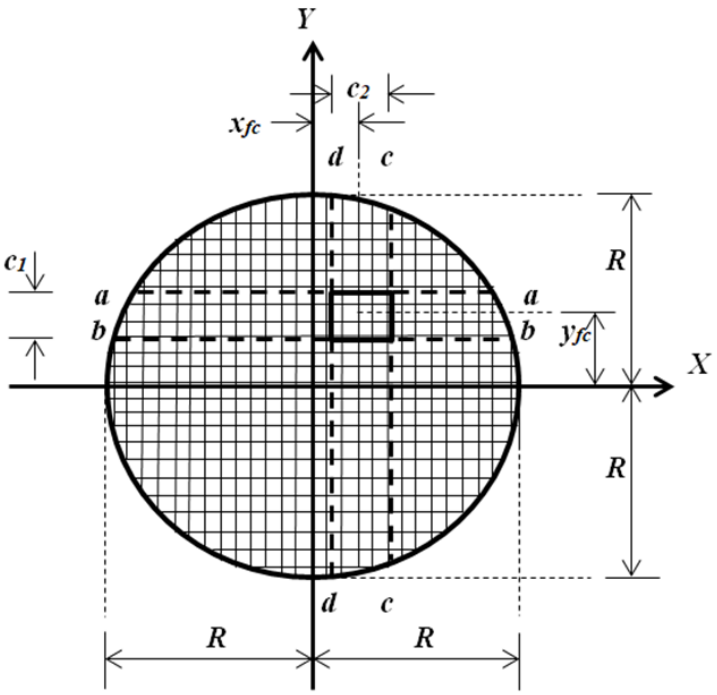

Fig. 1 Moments in the critical sections for an circular isolated footing with eccentric column

The general equation to estimate the soil pressure on the footing due to the factored loads and moments is (Luévanos-Rojas *et al.* 2024b)

$$\sigma_u(x,y) = \frac{P_u}{\pi R^2} + \frac{4\left(M_{xu} + P_u y_{fc}\right)y}{\pi R^4} + \frac{4\left(M_{yu} + P_u x_{fc}\right)x}{\pi R^4} \tag{1}$$

where: σ_u is the factored soil pressure on the footing (kN/m^2), R is the radius of the circular base (m), x_{fc} and y_{fc} are the coordinates where the column is located (m), x and y are the coordinates in the X and Y directions of the base (m), P_u is the factored axial load (kN)=1.2P_D (Dead load)+1.6P_L (Live load), M_{xu} is the factored moment on the X axis (kN-m)=1.2M_{xD} (Dead load moment on the X axis)+1.6M_{xL} (Live load moment on the X axis), M_{yu} is the factored moment on the Y axis (kN-m)=1.2M_{yD} (Dead load moment on the Y axis)+1.6M_{yL} (Live load moment on the Y axis) (ACI 318S-14 2014).

2.1.1 Factored moments

Fig. 1 presents the critical sections for the moments. The moments to be obtained in the critical sections appear on the *a*, *b*, *c* and *d* axes.

The moments M_{au} on the *a* axis, M_{bu} on the *b* axis, M_{cu} on the *c* axis, and M_{du} on the *d* axis are obtained by Luévanos-Rojas *et al.* (2024b)

$$M_{au} = -\int_{y_{fc}+\frac{c_1}{2}}^{R} \int_{-\sqrt{R^2-y^2}}^{\sqrt{R^2-y^2}} \sigma_u \left(y - y_{fc} - \frac{c_1}{2}\right) dxdy \tag{2}$$

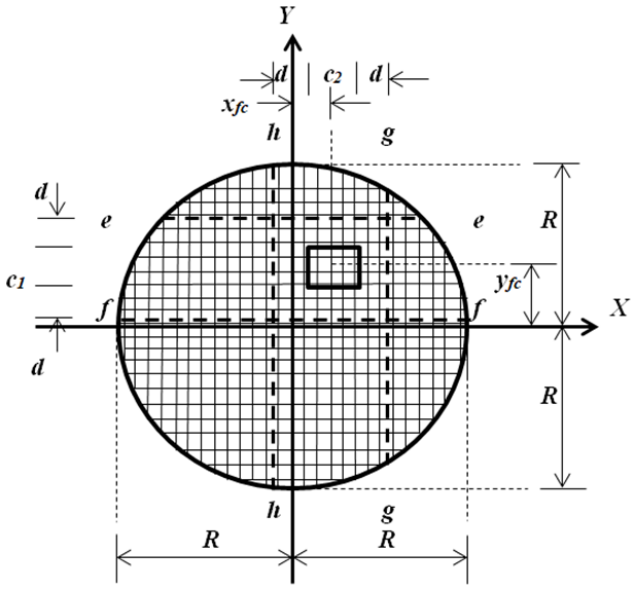

Fig. 2 Bending shears in the critical sections for a circular isolated footing with eccentric column

$$M_{bu}=\frac{P_u c_1}{2}+M_{xu}-\int_{y_{fc}-\frac{c_1}{2}}^{R}\int_{-\sqrt{R^2-y^2}}^{\sqrt{R^2-y^2}}\sigma_u\left(y-y_{fc}+\frac{c_1}{2}\right)dxdy \tag{3}$$

$$M_{cu}=-\int_{x_{fc}+\frac{c_2}{2}}^{R}\int_{-\sqrt{R^2-x^2}}^{\sqrt{R^2-x^2}}\sigma_u\left(x-x_{fc}-\frac{c_2}{2}\right)dydx \tag{4}$$

$$M_{du}=\frac{P_u c_2}{2}+M_{yu}-\int_{x_{fc}-\frac{c_2}{2}}^{R}\int_{-\sqrt{R^2-x^2}}^{\sqrt{R^2-x^2}}\sigma_u\left(x-x_{fc}+\frac{c_2}{2}\right)dydx \tag{5}$$

where: c_1 is the side of the column in the Y direction (m), c_2 is the side of the column in the X direction (m).

2.1.2 Factored bending shears

Fig. 2 shows the critical sections for bending shears. The bending shears to be obtained in the critical sections appear on the *e*, *f*, *g* and *h* axes.

The bending shears V_{eu} on the *e* axis, V_{fu} on the *f* axis, V_{gu} on the *g* axis, and V_{hu} on the *h* axis are obtained by Luévanos-Rojas *et al.* (2024b)

$$V_{eu}=-\int_{y_{fc}+\frac{c_1}{2}+d}^{R}\int_{-\sqrt{R^2-y^2}}^{\sqrt{R^2-y^2}}\sigma_u dxdy \tag{6}$$

$$V_{uf}=P_u-\int_{y_{fc}-\frac{c_1}{2}-d}^{R}\int_{-\sqrt{R^2-y^2}}^{\sqrt{R^2-y^2}}\sigma_u dxdy \tag{7}$$

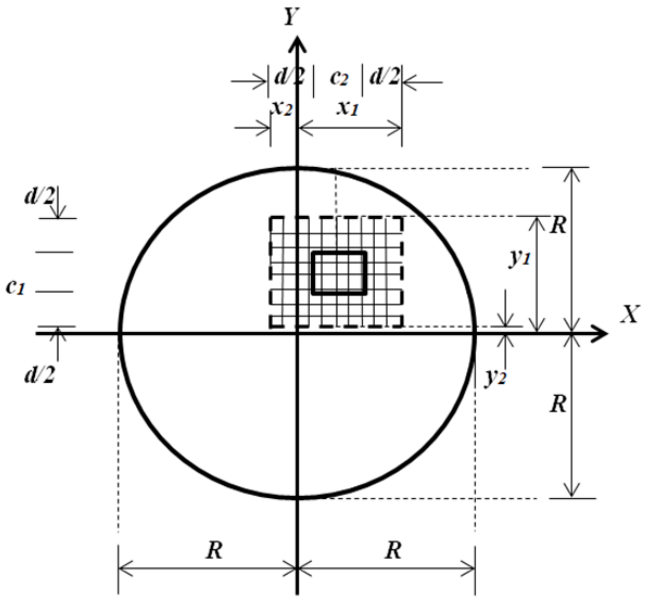

Fig. 3 Punching shear in the critical perimeter for an circular isolated footing with eccentric column

$$V_{gu} = -\int_{x_{fc}+\frac{c_2}{2}+d}^{R} \int_{-\sqrt{R^2-x^2}}^{\sqrt{R^2-x^2}} \sigma_u dydx \tag{8}$$

$$V_{hu} = P_u - \int_{x_{fc}-\frac{c_2}{2}-d}^{R} \int_{-\sqrt{R^2-x^2}}^{\sqrt{R^2-x^2}} \sigma_u dydx \tag{9}$$

2.1.3 Factored punching shear

Fig. 3 shows the critical perimeter for the punching shear. The punching shear to be obtained in the critical perimeter appears on the *Y* direction from y_2 to y_1 and in the *X* direction from x_2 to x_1.

The punching shear V_{eu} on the critical perimeter is obtained by Luévanos-Rojas *et al.* (2024b)

$$V_{pu} = P_u - \int_{y_2}^{y_1} \int_{x_2}^{x_1} \sigma_u dxdy \tag{10}$$

where: $y_2=y_{fc}-c_1/2-d/2$, $y_1=y_{fc}+c_1/2+d/2$, $x_2=x_{fc}-c_2/2-d/2$, $x_1=x_{fc}+c_2/2+d/2$ (When the critical perimeter is located inside the footing), When the critical perimeter is located in a portion outside the footing, the perimeter that is located inside the footing must be considered.

2.2 Case II: Area works partially under compression

The general equation to estimate the soil pressure on the footing due to the factored maximum pressure is obtained (Luévanos-Soto *et al.* 2024)

$$\sigma_z(x,y) = \frac{\sigma_{umax}(x\,sin\,\alpha + y\,cos\,\alpha - y_0)}{(R-y_0)} \tag{11}$$

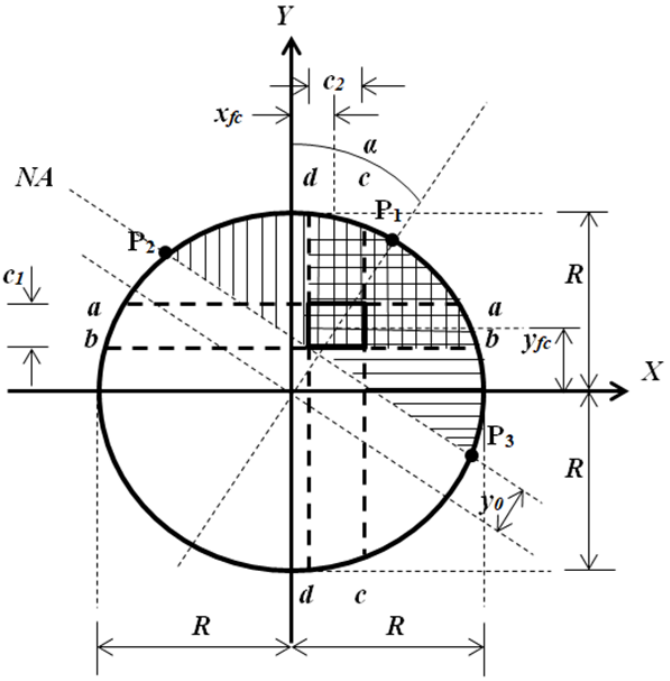

Fig. 4 Moments in the critical sections for a circular isolated footing with eccentric column

where: σ_z is the factored soil pressure anywhere on the base (kN/m^2), σ_{umax} is the factored maximum pressure (kN/m^2), x and y are the coordinates in the X and Y directions of the base (m), y_0 is the distance from the center of the footing to the neutral axis measured on the axis where the resultant moment appears (m), α is the inclination angle of the resultant moment with respect to the Y axis (rad).

2.2.1 Factored moments

Fig. 4 shows the critical sections for the moments. The points P_2 and P_3 have zero pressure, i.e., the straight line joining the points P_2 and P_3 is called the neutral axis and the point P_1 has the maximum pressure.

The moments are obtained in the critical sections that appear on the a, b, c and d axes.

M_{au} on the a axis is estimated through the pressure volume formed by σ_z, the surface delimited by the a axis, the neutral axis and the circumference, this is with respect to the a axis

$$M_{au} = -\int_{y_0 \cos\alpha+\sqrt{R^2-y_0^2}\sin\alpha}^{R} \int_{-\sqrt{R^2-y^2}}^{\sqrt{R^2-y^2}} \sigma_z \left(y - y_{fc} - \frac{c_1}{2}\right) dxdy - \int_{y_{fc}+\frac{c_1}{2}}^{y_0 \cos\alpha+\sqrt{R^2-y_0^2}\sin\alpha} \int_{\frac{y_0-y\cos\alpha}{\sin\alpha}}^{\sqrt{R^2-y^2}} \sigma_z \left(y - y_{fc} - \frac{c_1}{2}\right) dxdy \tag{12}$$

M_{bu} on the b axis is obtained through P_u multiplied by $c_1/2$ plus M_{xu} minus the pressure volume formed by σ_z, the surface delimited by the b axis, the neutral axis and the circumference, this pressure is with respect to the b axis

$$M_{bu} = \frac{P_u c_1}{2} + M_{xu} - \int_{y_0 \cos\alpha + \sqrt{R^2 - {y_0}^2}\sin\alpha}^{R} \int_{-\sqrt{R^2-y^2}}^{\sqrt{R^2-y^2}} \sigma_z \left(y - y_{fc} + \frac{c_1}{2}\right) dxdy - \int_{y_{fc}-\frac{c_1}{2}}^{y_0 \cos\alpha + \sqrt{R^2-{y_0}^2}\sin\alpha} \int_{\frac{y_0 - y\cos\alpha}{\sin\alpha}}^{\sqrt{R^2-y^2}} \sigma_z \left(y - y_{fc} + \frac{c_1}{2}\right) dxdy \quad (13)$$

M_{cu} on the c axis is estimated through the pressure volume formed by σ_z, the surface delimited by the c axis, the neutral axis and the circumference, this pressure is with respect to the c axis

$$M_{cu} = -\int_{y_0 \sin\alpha + \sqrt{R^2-{y_0}^2}\cos\alpha}^{R} \int_{-\sqrt{R^2-x^2}}^{\sqrt{R^2-x^2}} \sigma_z \left(x - x_{fc} - \frac{c_2}{2}\right) dydx - \int_{x_{fc}+\frac{c_2}{2}}^{y_0 \sin\alpha + \sqrt{R^2-{y_0}^2}\cos\alpha} \int_{\frac{y_0 - x\sin\alpha}{\cos\alpha}}^{\sqrt{R^2-x^2}} \sigma_z \left(x - x_{fc} - \frac{c_2}{2}\right) dydx \quad (14)$$

M_{du} on the d axis is obtained through P_u multiplied by $c_2/2$ plus M_{yu} minus the pressure volume formed by σ_z, the surface delimited by the d axis, the neutral axis and the circumference, this pressure is with respect to the d axis

$$M_{du} = \frac{P_u c_2}{2} + M_{yu} - \int_{y_0 \sin\alpha + \sqrt{R^2-{y_0}^2}\cos\alpha}^{R} \int_{-\sqrt{R^2-x^2}}^{\sqrt{R^2-x^2}} \sigma_z \left(x - x_{fc} + \frac{c_2}{2}\right) dydx - \int_{x_{fc}-\frac{c_2}{2}}^{y_0 \sin\alpha + \sqrt{R^2-{y_0}^2}\cos\alpha} \int_{\frac{y_0 - x\sin\alpha}{\cos\alpha}}^{\sqrt{R^2-x^2}} \sigma_z \left(x - x_{fc} + \frac{c_2}{2}\right) dydx \quad (15)$$

2.2.2 Factored bending shears

Fig. 5 presents the critical sections for the bending shears. The bending shears are obtained in the critical sections that appear on the *e*, *f*, *g* and *h* axes.

V_{eu} on the e axis is estimated through the pressure volume formed by σ_z, the surface delimited by the e axis, the neutral axis and the circumference

$$V_{eu} = -\int_{y_0 \cos\alpha + \sqrt{R^2-{y_0}^2}\sin\alpha}^{R} \int_{-\sqrt{R^2-y^2}}^{\sqrt{R^2-y^2}} \sigma_z dxdy - \int_{y_{fc}+\frac{c_1}{2}+d}^{y_0 \cos\alpha + \sqrt{R^2-{y_0}^2}\sin\alpha} \int_{\frac{y_0 - y\cos\alpha}{\sin\alpha}}^{\sqrt{R^2-y^2}} \sigma_z dxdy \quad (16)$$

V_{fu} on the f axis is estimated through P_u minus the pressure volume formed by σ_z, the surface delimited by the f axis, neutral axis and the circumference

$$V_{fu} = P_u - \int_{y_0 \cos\alpha + \sqrt{R^2-{y_0}^2}\sin\alpha}^{R} \int_{-\sqrt{R^2-y^2}}^{\sqrt{R^2-y^2}} \sigma_z dxdy - \int_{y_{fc}-\frac{c_1}{2}-d}^{y_0 \cos\alpha + \sqrt{R^2-{y_0}^2}\sin\alpha} \int_{\frac{y_0 - y\cos\alpha}{\sin\alpha}}^{\sqrt{R^2-y^2}} \sigma_z dxdy \quad (17)$$

V_{gu} on the g axis is estimated through the pressure volume formed by σ_z, the surface delimited by the g axis, the neutral axis and the circumference

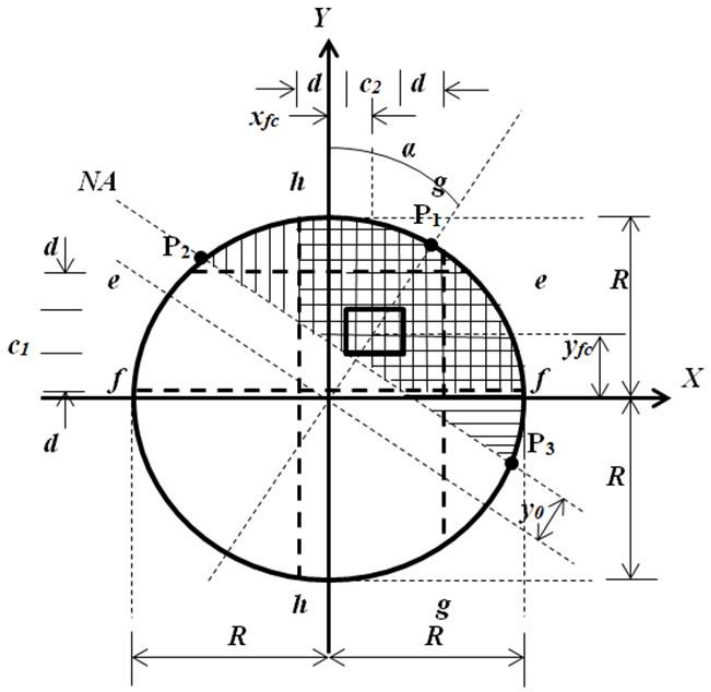

Fig. 5 Bending shears in the critical sections for a circular isolated footing with eccentric column

$$V_{gu} = -\int_{y_0 \sin\alpha+\sqrt{R^2-y_0^2}\cos\alpha}^{R} \int_{-\sqrt{R^2-x^2}}^{\sqrt{R^2-x^2}} \sigma_z dydx - \int_{x_{fc}+\frac{c_2}{2}+d}^{y_0 \sin\alpha+\sqrt{R^2-y_0^2}\cos\alpha} \int_{\frac{y_0-x\sin\alpha}{\cos\alpha}}^{\sqrt{R^2-x^2}} \sigma_z dydx \quad (18)$$

V_{hu} on the h axis is estimated through P_u minus the pressure volume formed by σ_z, the surface delimited by the h axis, the neutral axis and the circumference

$$V_{hu} = P_u - \int_{y_0 \sin\alpha+\sqrt{R^2-y_0^2}\cos\alpha}^{R} \int_{-\sqrt{R^2-x^2}}^{\sqrt{R^2-x^2}} \sigma_z dydx - \int_{x_{fc}-\frac{c_2}{2}-d}^{y_0 \sin\alpha+\sqrt{R^2-y_0^2}\cos\alpha} \int_{\frac{y_0-x\sin\alpha}{\cos\alpha}}^{\sqrt{R^2-x^2}} \sigma_z dydx \quad (19)$$

2.2.3 Factored punching shear

Fig. 6 presents the critical perimeter for the punching shear. The punching shear is obtained in the critical perimeter that appears on the Y direction from y_2 to y_1 and in the X direction from x_2 to x_1.

V_{pu} is estimated through P_u minus the pressure volume formed by σ_z, the surface delimited on the Y direction from y_{fc}-$c_1/2$-$d/2$ to y_{fc}+$c_1/2$+$d/2$ and in the X direction from x_{fc}–$c_2/2$-$d/2$ to x_{fc}+$c_2/2$+$d/2$

$$V_{pu} = P_u - \int_{y_2}^{y_1} \int_{x_2}^{x_1} \sigma_z dxdy \quad (20)$$

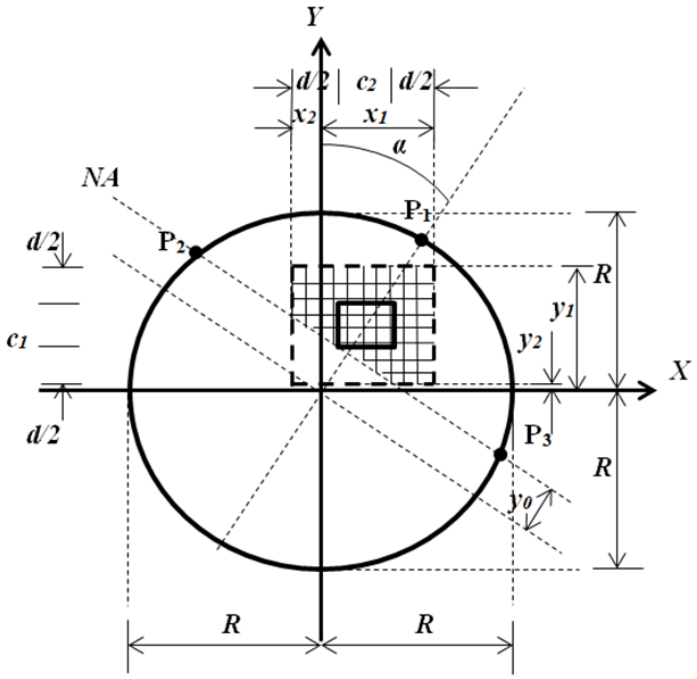

Fig. 6 Punching shear in the critical perimeter for a circular isolated footing with eccentric column

where: $y_2=y_{fc}-c_1/2-d/2$, $y_1=y_{fc}+c_1/2+d/2$, $x_2=x_{fc}-c_2/2-d/2$, $x_1=x_{fc}+c_2/2+d/2$ (When the critical perimeter is located inside the footing), When the critical perimeter is located in a portion outside the footing, the perimeter that is located inside the footing must be considered. Also, if the neutral axis crosses part of the critical perimeter, only the shaded part must be considered as seen in Fig. 6.

2.2.4 Objective function

The minimum cost is

$$C_{min} = V_c C_c + V_s \gamma_s C_s \tag{21}$$

where: C_{min}=minimum cost, C_c=cost of concrete, V_c=volume of concrete, C_s=cost of steel, V_s=volume of steel, γ_s=density of steel=78 kN/m^3.

The construction of the steel reinforcement of the footing is as follows: A square or rectangular grid (X and Y directions) and a circular perimeter ring at a distance r (concrete cover) from the free end of the footing inwards.

The total length of the steel bars in the X direction is obtained as follows

$$L_x = 2R + 4 \sum_{j=1}^{(n_x-3)/2} \sqrt{R^2-(js_x)^2} \tag{22}$$

where s_x is the space between the reinforcing steel bars in the X direction, n_x is the number of rods in the X direction.

The total length of the steel bars in the Y direction is obtained as follows

$$L_y = 2R + 4\sum_{i=1}^{(n_y-3)/2}\sqrt{R^2-\left(is_y\right)^2} \tag{23}$$

where s_y is the space between the reinforcing steel bars in the Y direction, n_y is the number of rods in the Y direction.

Length of the circumferential steel bar "L_c" is as follows

$$L_c = 2\pi(R-r) \tag{24}$$

The total volume of steel is

$$V_s = a_s\left(L_y + L_x + L_c\right) \tag{25}$$

where: a_s is the cross-sectional area of the rod used and is assumed to be the same in both directions.

The volume of concrete is

$$V_c = \pi R^2(d+r) - a_s\left(L_y + L_x + L_c\right) \tag{26}$$

Substituting the Eqs. (22), (23) and (24) into Eq. (21) is given

$$C_{min} = \left[\pi R^2(d+r) - a_s\left(L_y + L_x + L_c\right)\right]C_c + \left[a_s\left(L_y + L_x + L_c\right)\right]\gamma_s C_s \tag{27}$$

Substituting $\alpha=\gamma_s C_s/C_c \rightarrow \gamma_s C_s=\alpha C_c$ into substituting Eq. (27) is given

$$C_{min} = \left[\left(4R + 4\sum_{j=1}^{(n_x-3)/2}\sqrt{R^2-(js_x)^2} + 4\sum_{i=1}^{(n_y-3)/2}\sqrt{R^2-\left(is_y\right)^2} + 2\pi(R-r)\right)(\alpha-1)a_s + \pi R^2(d+r)\right]C_c \tag{28}$$

2.2.5 Constraint functions

The adjusted equations for the design of circular footings according to the standard code are shown below (ACI 318S-14 2014).

For moments

$$|M_{au}|, |M_{bu}|, |M_{cu}|, |M_{du}| \leq \emptyset_f f_y d A_s\left(1-\frac{A_s f_y}{1.7 b_w d f'_c}\right) \tag{29}$$

The reinforcing areas in both directions are obtained as follows

$$A_{sya} = \rho_x b_{wxa} d \tag{30}$$

$$A_{syb} = \rho_x b_{wxb} d \tag{31}$$

$$A_{sxc} = \rho_y b_{wyc} d \tag{32}$$

$$A_{sxd} = \rho_y b_{wyd} d \tag{33}$$

where: b_{wxa}, b_{wxb}, b_{wyc} and b_{wyd} are obtained as follows

$$b_{wxa} = 2\sqrt{R^2 - \left(y_{fc} + c_1/2\right)^2} \tag{34}$$

$$b_{wxb} = 2\sqrt{R^2 - \left(y_{fc} - c_1/2\right)^2} \tag{35}$$

$$b_{wyc} = 2\sqrt{R^2 - \left(x_{fc} + c_2/2\right)^2} \tag{36}$$

$$b_{syd} = 2\sqrt{R^2 - \left(x_{fc} - c_2/2\right)^2} \tag{37}$$

where: A_s and b_w for M_{au} are A_{sya} and b_{wxa}, for M_{bu} are A_{syb} and b_{wxb}, for M_{cu} are A_{sxc} and b_{wyc}, for M_{du} are A_{sxd} and b_{wyd}, f_y is the specified yield strength of reinforcement of steel, f'_c is the specified compressive strength of the concrete at 28 days, A_{sx} is the steel area in the *X* directions, A_{sy} is the steel area in the *Y* directions, $\emptyset_f$=0.90 (bending strength reduction factor).

For bending shears

$$|V_{eu}|, |V_{fu}|, |V_{gu}|, |V_{hu}| \leq 0.17\emptyset_v \sqrt{f'_c} b_{ws} d \tag{38}$$

where: b_{wsxe}, b_{wsxf}, b_{wsyg} and b_{wsyh} are obtained as follows

$$b_{wsxe} = 2\sqrt{R^2 - \left(y_{fc} + c_1/2 + d\right)^2} \tag{39}$$

$$b_{wsxf} = 2\sqrt{R^2 - \left(y_{fc} - c_1/2 - d\right)^2} \tag{40}$$

$$b_{wsyg} = 2\sqrt{R^2 - \left(x_{fc} + c_2/2 + d\right)^2} \tag{41}$$

$$b_{wsyh} = 2\sqrt{R^2 - \left(x_{fc} - c_2/2 - d\right)^2} \tag{42}$$

where: b_{ws} for V_{eu} is b_{wsxe}, for V_{fu} is b_{wsxf}, for V_{gu} is b_{wsyg}, for V_{hu} is b_{wsyh}, $\emptyset_v$=0.85 (shear strength reduction factor).

For punching shear

$$|V_{pu}| \leq \begin{cases} 0.17\emptyset_v \left(1 + \dfrac{2}{\beta_c}\right) \sqrt{f'_c} b_0 d \\ 0.083\emptyset_v \left(\dfrac{\alpha_s d}{b_0} + 2\right) \sqrt{f'_c} b_0 d \\ 0.33\emptyset_v \sqrt{f'_c} b_0 d \end{cases} \tag{43}$$

where: β_c=long side of column/short side of column, b_0 is the critical perimeter, α_s=20 (corner column), α_s=30 (edge column), and α_s=40 (interior column).

For percentages of steel

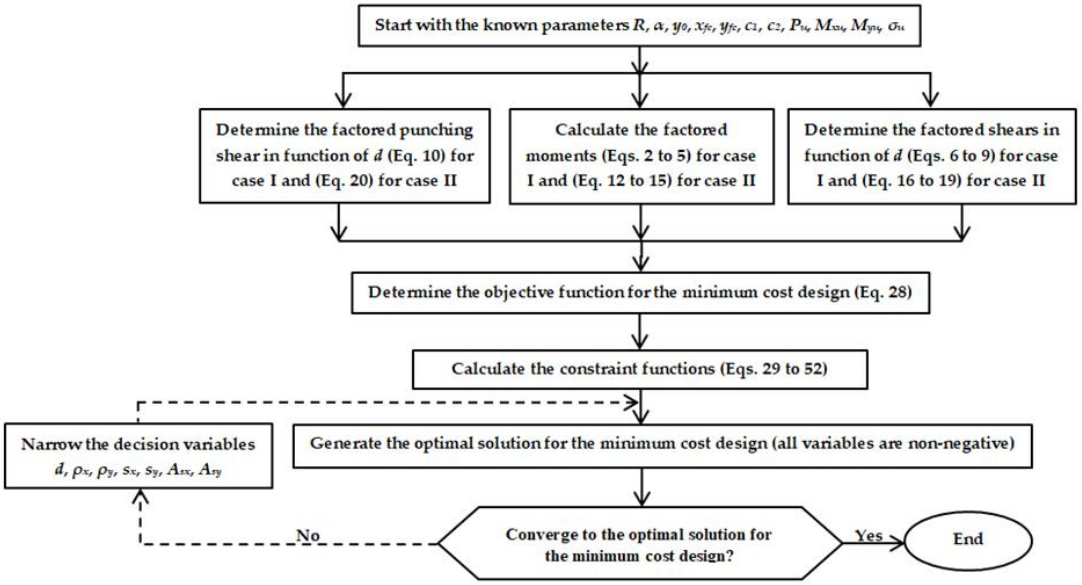

Fig. 7 Flowchart for the minimum cost design of a circular isolated footing with eccentric column

$$\rho_x, \rho_y \leq 0.75\left[\frac{0.85\beta_1 f'_c}{f_y}\left(\frac{600}{600+f_y}\right)\right] \tag{44}$$

$$\rho_x, \rho_y \geq \begin{cases} \dfrac{0.25\sqrt{f'_c}}{f_y} \\ \dfrac{1.4}{f_y} \end{cases} \tag{45}$$

$$0.65 \leq \beta_1 = \left(1.05 - \frac{f'_c}{140}\right) \leq 0.85 \tag{46}$$

where: β_1 is the factor relating the depth of the equivalent rectangular compressive stress block to the depth of the neutral axis.

For steel areas

$$A_{sy} \geq \begin{cases} A_{sya} = \rho_y b_{wxa} d \\ A_{syb} = \rho_y b_{wxb} d \end{cases} \tag{47}$$

$$A_{sx} \geq \begin{cases} A_{sxc} = \rho_x b_{wyc} d \\ A_{sxd} = \rho_x b_{wyd} d \end{cases} \tag{48}$$

For number of rods

$$n_y = \frac{A_{sy}}{a_s} \tag{49}$$

$$n_x = \frac{A_{sx}}{a_s} \tag{50}$$

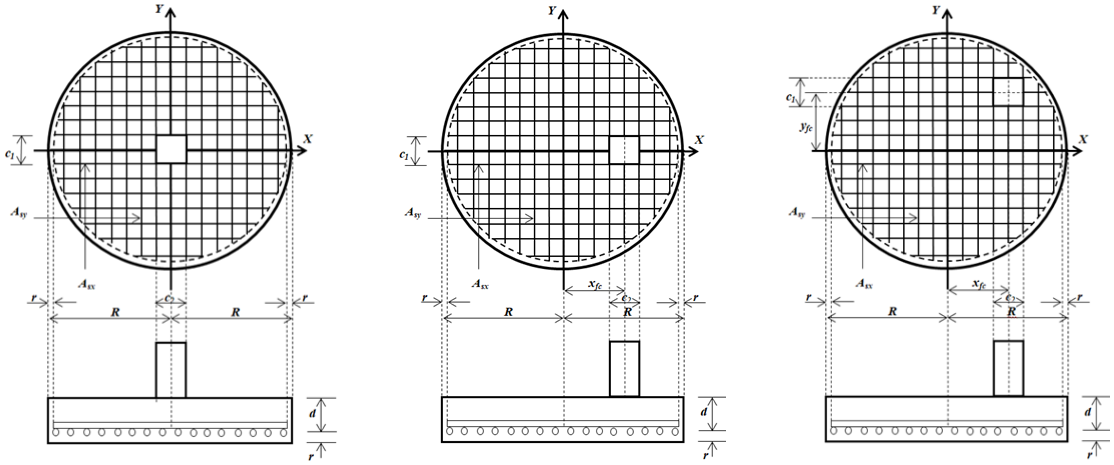

(a) Example 1 (b) Example 2 (c) Example 3

Fig. 8 Three examples for the minimum cost design

Table 1 Example 1: x_{fc}=0 and y_{fc}=0

Case	Proposed solution			σ_u (kN/m^2)	A_{sx} (cm^2)	A_{sy} (cm^2)	s_x (cm)	s_y (cm)	d (cm)	ρ_x	ρ_y	C_{min} (USD)
	R (m)	y_0 (m)	A_{min} (m^2)									
Example 1.1: P_D=300 kN, P_L=200 kN, P_u=680 kN, M_{yD}=60 kN-m, M_{yL}=40 kN-m, M_{yu}=136 kN-m, M_{xD}=180 kN-m, M_{xL}=120 kN-m, M_{xu}=408 kN-m, M_{Ru}=430.07 kN-m, α=0.3217 Rad												
1	1.45	-0.58	6.61	309.93	26.28	32.34	13.87	11.27	27.5	0.00333	0.00410	3.53C_c
2	1.55	-0.73	7.55	253.32	28.11	33.59	13.87	11.61	27.5	0.00333	0.00398	4.01C_c
3	1.70	-0.97	9.08	193.91	30.95	35.71	13.87	12.02	27.5	0.00333	0.00384	4.26C_c
4	1.95	-1.36	11.95	133.08	35.53	39.54	13.87	12.46	27.5	0.00333	0.00371	6.30C_c
Example 1.2: P_D=300 kN, P_L=200 kN, P_u=680 kN, M_{yD}=60 kN-m, M_{yL}=40 kN-m, M_{yu}=136 kN-m, M_{xD}=120 kN-m, M_{xL}=80 kN-m, M_{xu}=272 kN-m, M_{Ru}=304.11 kN-m, α=0.4636 Rad												
1	1.30	-0.82	5.31	311.16	23.53	23.53	13.87	13.87	27.5	0.00333	0.00333	2.72C_c
2	1.40	-0.98	6.16	254.56	25.37	25.37	13.87	13.87	27.5	0.00333	0.00333	3.18C_c
3	1.55	-1.22	7.55	194.78	28.11	28.11	13.87	13.87	27.5	0.00333	0.00333	3.89C_c
4	1.80	-1.62	10.18	133.20	32.78	32.78	13.87	13.87	27.5	0.00333	0.00333	5.27C_c
Example 1.3: P_D=300 kN, P_L=200 kN, P_u=680 kN, M_{yD}=60 kN-m, M_{yL}=40 kN-m, M_{yu}=136 kN-m, M_{xD}=90 kN-m, M_{xL}=60 kN-m, M_{xu}=204 kN-m, M_{Ru}=245.18 kN-m, α=0.5880 Rad												
1	1.20	-0.89	4.52	328.69	21.70	21.70	13.87	13.87	27.5	0.00333	0.00333	2.36C_c
2	1.30	-1.05	5.31	266.22	23.53	23.53	13.87	13.87	27.5	0.00333	0.00333	2.72C_c
3	1.45	-1.30	6.61	200.82	26.28	26.28	13.87	13.87	27.5	0.00333	0.00333	3.38C_c
4	1.75	*	9.62	128.93	31.87	31.87	13.87	13.87	27.5	0.00333	0.00333	5.00C_c

For space between bars

$$s_y = \frac{b_{wx} a_s}{A_{sy}} \tag{51}$$

$$s_x = \frac{b_{wy} a_s}{A_{sx}} \tag{52}$$

Table 2 Example 2: x_{fc}=1.50 m and y_{fc}=0

Case	Proposed solution			σ_u	A_{sx}	A_{sy}	s_x	s_y	d	ρ_x	ρ_y	C_{min}
	R (m)	y_0 (m)	A_{min} (m^2)	(kN/m^2)	(cm^2)	(cm^2)	(cm)	(cm)	(cm)			(USD)
Example 2.1: P_D=480 kN, P_L=320 kN, P_u=1088 kN, M_{yD}=-480 kN-m, M_{yL}=-320 kN-m, M_{yu}=-1088 kN-m, M_{xD}=300 kN-m, M_{xL}=200 kN-m, M_{xu}=680 kN-m, M_{Ru}=870.82 kN-m, α=0.6747 Rad												
1	1.80	-0.62	10.18	326.38	70.33	44.74	25.81	28.22	37.5	0.00753	0.00333	$7.44C_c$
2	1.95	-0.85	11.95	254.54	84.66	53.92	23.23	27.36	32.5	0.00895	0.00428	$8.52C_c$
3	2.15	-1.15	14.52	190.57	86.30	57.16	25.14	30.33	32.5	0.00776	0.00411	$10.49C_c$
4	2.45	-1.62	18.86	131.64	89.88	62.14	27.53	33.86	32.5	0.00666	0.00392	$12.94C_c$
Example 2.2: P_D=480 kN, P_L=320 kN, P_u=1088 kN, M_{yD}=-420 kN-m, M_{yL}=-280 kN-m, M_{yu}=-952 kN-m, M_{xD}=300 kN-m, M_{xL}=200 kN-m, M_{xu}=680 kN-m, M_{Ru}=961.67 kN-m, α=0.7854 Rad												
1	1.85	-0.46	10.75	335.89	59.76	45.98	31.22	29.00	37.5	0.00606	0.00333	$7.79C_c$
2	2.00	-0.68	12.57	258.60	72.27	53.93	27.92	28.58	32.5	0.00731	0.00417	$8.55C_c$
3	2.20	-0.99	15.21	191.33	74.64	56.97	29.75	31.59	32.5	0.00647	0.00400	$10.30C_c$
4	2.50	-1.47	19.63	130.29	78.86	61.39	32.02	41.13	32.5	0.00487	0.00379	$12.92C_c$
Example 2.3: P_D=480 kN, P_L=320 kN, P_u=1088 kN, M_{yD}=-360 kN-m, M_{yL}=-240 kN-m, M_{yu}=-816 kN-m, M_{xD}=300 kN-m, M_{xL}=200 kN-m, M_{xu}=680 kN-m, M_{Ru}=1062.19 kN-m, α=0.8761 Rad												
1	1.95	-0.30	11.95	325.79	59.62	52.61	33.00	28.04	32.5	0.00630	0.00417	$7.90C_c$
2	2.05	-0.48	13.20	268.83	60.88	53.91	33.98	29.81	32.5	0.00591	0.00407	$8.57C_c$
3	2.25	-0.82	15.90	194.05	63.71	56.77	35.65	32.78	32.5	0.00534	0.00390	$10.33C_c$
4	2.55	-1.29	20.43	135.38	68.99	63.06	37.33	35.30	32.5	0.00484	0.00382	$13.03C_c$

The flowchart to obtain the minimum cost design of a circular isolated footing with eccentric column for the two cases is shown in Fig. 7.

3. Numerical examples

Tables 1, 2 and 3 show the minimum cost design of a circular isolated footing under biaxial bending based on the same three examples presented in the minimum area paper that appear in Tables 2, 3 and 4 of Luévanos-Soto *et al.* (2024).

Fig. 8 shows the three examples for the minimum cost design of a circular isolated footing.

Fig. 8(a) shows the example 1 (x_{fc}=0 and y_{fc}=0). Fig. 8(b) presents the example 2 (x_{fc}=1.50 m and y_{fc}=0). Fig. 8(c) shows the example 3 (x_{fc}=1.50 m and y_{fc}=1.50 m).

The general data for design of the three examples are c_1=c_2=0.40 m, r=7.5 cm, a_s=1.27 cm^2 (1Ø1/2"), f'_c=21 MPa, f_y=420 MPa and α=90.

Table 1 shows the example 1 for a column located in x_{fc}=0 and y_{fc}=0 (center of the base).

Table 2 presents the example 2 for a column located in x_{fc}=1.50 m and y_{fc}=0.

Table 3 shows the example 3 for a column located in x_{fc}=1.50 m and y_{fc}=1.50 m.

4. Results

This model can be checked as follows.

Table 3 Example 3: x_{fc}=1.50 m and y_{fc}=1.50 m

Case	Proposed solution			σ_u	A_{sx}	A_{sy}	s_x	s_y	d	ρ_x	ρ_y	C_{min}
	R (m)	y_0 (m)	A_{min} (m^2)	(kN/m^2)	(cm^2)	(cm^2)	(cm)	(cm)	(cm)			(USD)
Example 3.1: P_D=480 kN, P_L=320 kN, P_u=1088 kN, M_{yD}=-480 kN-m, M_{yL}=-320 kN-m, M_{yu}=-1088 kN-m, M_{xD}=300 kN-m, M_{xL}=200 kN-m, M_{xu}=680 kN-m, M_{Ru}=2375.14 kN-m, α=0.2311 Rad												
1	3.05	1.06	29.22	311.80	91.04	59.75	30.74	46.84	32.5	0.00507	0.00333	18.49C_c
2	3.15	0.87	31.17	255.25	94.01	62.13	30.96	46.84	32.5	0.00504	0.00333	19.53C_c
3	3.30	0.63	34.21	199.41	97.66	65.70	31.51	46.84	32.5	0.00495	0.00333	21.52C_c
4	3.60	0.16	40.72	134.07	104.55	72.63	32.54	46.84	32.5	0.00479	0.00333	25.44C_c
Example 3.2: P_D=480 kN, P_L=320 kN, P_u=1088 kN, M_{yD}=-420 kN-m, M_{yL}=-280 kN-m, M_{yu}=-952 kN-m, M_{xD}=300 kN-m, M_{xL}=200 kN-m, M_{xu}=680 kN-m, M_{Ru}=2409.93 kN-m, α=0.2861 Rad												
1	3.10	1.14	30.19	309.70	81.68	60.94	34.95	46.84	32.5	0.00446	0.00333	18.52C_c
2	3.20	0.91	32.17	249.49	85.17	63.32	34.82	46.84	32.5	0.00448	0.00333	19.56C_c
3	3.35	0.65	35.26	194.11	89.20	66.78	35.07	46.84	32.5	0.00445	0.00333	22.01C_c
4	3.65	0.17	41.85	130.76	96.47	73.82	35.84	46.84	32.5	0.00435	0.00333	25.91C_c
Example 3.3: P_D=480 kN, P_L=320 kN, P_u=1088 kN, M_{yD}=-360 kN-m, M_{yL}=-240 kN-m, M_{yu}=-816 kN-m, M_{xD}=300 kN-m, M_{xL}=200 kN-m, M_{xu}=680 kN-m, M_{Ru}=2451.77 kN-m, α=0.3393 Rad												
1	3.20	1.13	32.17	280.47	74.21	63.32	39.97	46.84	32.5	0.00390	0.00333	19.06C_c
2	3.25	1.00	33.18	249.48	76.08	64.51	39.72	46.84	32.5	0.00393	0.00333	19.98C_c
3	3.40	0.69	36.32	191.33	80.83	67.97	39.39	46.84	32.5	0.00396	0.00333	22.06C_c
4	3.70	0.20	43.01	128.49	88.37	75.01	39.76	46.84	32.5	0.00392	0.00333	25.98C_c

For moments on the *X* axis:

1.- Replacing $y_{fc}+c_1/2$ by $y_0\cos\alpha-\sqrt{R^2-{y_0}^2}\sin\alpha$ on the lower limit and $y-y_{fc}-c_1/2$ by y into Eq. (12) gives: M_{au}=0 (moment at the upper end according to Fig. 5).

2.- Replacing $y_{fc}+c_1/2$ by y_{fc} on the lower limit and $y-y_{fc}-c_1/2$ by $y-y_{fc}$ into Eq. (12) gives: M_{au} (moment in the center of the column), and replacing $y_{fc}-c_1/2$ by y_{fc} on the lower limit and $y-y_{fc}+c_1/2$ by $y-y_{fc}$ into Eq. (13) gives: M_{bu} (moment in the center of the column). Now, making M_{au}=M_{bu} and removing $P_u c_1/2$ gives: M_{xu} (moment acting at the center of the column).

For moments on the *Y* axis:

1.- Replacing $x_{fc}+c_2/2$ by $y_0\sin\alpha-\sqrt{R^2-{y_0}^2}\cos\alpha$ on the lower limit and $x-x_{fc}-c_2/2$ by x into Eq. (14) gives: M_{cu}=0 (moment at the far right according to Fig. 5).

2.- Replacing $x_{fc}+c_2/2$ by x_{fc} on the lower limit and $x-x_{fc}-c_2/2$ by $x-x_{fc}$ into Eq. (14) gives: M_{cu} (moment in the center of the column), and replacing $x_{fc}-c_2/2$ by x_{fc} on the lower limit and $x-x_{fc}+c_2/2$ by $x-x_{fc}$ into Eq. (15) gives: M_{du} (moment in the center of the column). Now, making M_{cu}=M_{du} and removing $P_u c_2/2$ gives: M_{yu} (moment acting at the center of the column).

For bending shears on the *X* axis:

1.- Replacing $y_{fc}+c_1/2+d$ by $y_0\cos\alpha-\sqrt{R^2-{y_0}^2}\sin\alpha$ in the lower limit of the second member and replacing $y_0\cos\alpha-\sqrt{R^2-{y_0}^2}\sin\alpha$ by R in the lower limit of the first member into Eq. (16) gives: V_{eu}=0 (bending shear at the upper end according to Fig. 6).

2.- Replacing $y_{fc}+c_1/2+d$ by y_{fc} on the lower limit into Eq. (16) gives: V_{eu} (bending shear

in the center of the column), and replacing $y_{fc} - c_1/2 - d$ by y_{fc} on the lower limit into Eq. (17) gives: V_{fu} (bending shear in the center of the column). Now, making $V_{eu}=V_{fu}$ gives: P_u (bending shear acting at the center of the column).

For bending shears in the *Y* axis:

1.- Replacing $x_{fc} + c_2/2 + d$ by $y_0 \sin\alpha - \sqrt{R^2 - y_0{}^2}\cos\alpha$ in the lower limit of the second member and replacing $y_0 \sin\alpha - \sqrt{R^2 - y_0{}^2}\cos\alpha$ by R in the lower limit of the first member into Eq. (18) gives: $V_{gu}=0$ (bending shear at the far right according to Fig. 6).

2.- Replacing $x_{fc} + c_2/2 + d$ by x_{fc} on the lower limit into Eq. (18) gives: V_{gu} (bending shear in the center of the column), and replacing $x_{fc} - c_2/2 - d$ by x_{fc} on the lower limit into Eq. (19) gives: V_{hu} (bending shear in the center of the column). Now, making $V_{gu}=V_{hu}$ gives: P_u (bending shear acting at the center of the column).

Table 1 presents the following for Example 1 ($x_{fc}=0$ and $y_{fc}=0$): When σ_u decreases, R, y_0 (absolute value) except in example 1.3.4 where the area works completely in compression, A_{min}, A_{sx}, A_{sy} and C_{min} increase, s_x, s_y (except in example 1 where it tends to increase), d, ρ_x and ρ_y (except in example 1 where it tends to decrease) are same.

Table 2 presents the following for Example 2 ($x_{fc}=1.50$ and $y_{fc}=0$): When σ_u decreases, R, y_0 (absolute value), A_{min}, A_{sx}, A_{sy} and C_{min} increase, s_x and s_y decrease until example 2.1.2 for example 1 and subsequently increase, for example 2 they decrease until example 2.2.2 and subsequently increase, and for example 3 they increase, ρ_x and ρ_y increase until example 2.1.2 for example 1 and subsequently decrease, for example 2 they increase until example 2.2.2 and subsequently decrease, and for example 3 they decrease, d is the same for all examples (except in examples 2.1.1 and 2.2.1 where is greater).

Table 3 shows the following for Example 3 ($x_{fc}=1.50$ and $y_{fc}=1.50$): When σ_u decreases, R, A_{min}, A_{sx}, A_{sy} and C_{min} increase, y_0 decreases, ρ_x decreases for example 1, for example 2 they increase until example 3.2.2 and subsequently decrease, and for example 3 they increase until example 3.3.3 and subsequently decrease, d, s_y and ρ_y are same.

Also, a comparison is made between the MPLR (model proposed by Luévanos-Rojas *et al.* 2024b) against the NM (new model) proposed in this paper.

Tables 4 and 5 presents the results of Example 1 of the MPLR against the NM for P_D=800 kN and P_L=700 kN (Example 1A), P_D=700 kN and P_L=600 kN (Example 1B), P_D=600 kN and P_L=500 kN (Example 1C), P_D=500 kN and P_L=400 kN (Example 1D), M_{xD}=300 kN-m, M_{xL}=200 kN-m, M_{yD}=200 kN-m, M_{yL}=100 kN-m, x_{fc}=0 m, y_{fc}=0 m, $c_1=c_2$=0.50 m, r=0.075 m, a_s=5.07 cm^2 (1Ø1”), σ_{max}=200 kN/m^2, f'_c=21 MPa, f_y=420 MPa and α=90. Table 4 shows the minimum area and Table 5 presents the minimum cost design.

Tables 6 and 7 show the results of Example 2 of the MPLR against the NM for P_D=800 kN and P_L=600 kN (Example 2A), P_D=700 kN and P_L=500 kN (Example 2B), P_D=600 kN and P_L=400 kN (Example 2C), P_D=500 kN and P_L=300 kN (Example 2D), M_{xD}=300 kN-m, M_{xL}=200 kN-m, M_{yD}=-500 kN-m, M_{yL}=-500 kN-m, x_{fc}=R/2 m, y_{fc}=0 m, $c_1=c_2$=0.50 m, r=0.075 m, a_s=5.07 cm^2 (1Ø1”), σ_{max}=200 kN/m^2, f'_c=21 MPa, f_y=420 MPa and α=90. Table 6 shows the minimum area and Table 7 presents the minimum cost design.

Table 4 of the example 1 ($x_{fc}=0$ and $y_{fc}=0$) for minimum area of the MPLR show the following: the smallest values for R and A_{min} are presented in the MPLR because the NM does not present a solution for the two first examples, and for the last two examples the NM governs.

Table 5 of the example 1 ($x_{fc}=0$ and $y_{fc}=0$) for minimum cost design of the MPLR show the following: the smallest values for A_{sx}, A_{sy}, d and C_{min} are presented in the MPLR because the NM

Table 4 Minimum area of Example 1 of the MPLR against the NM: x_{fc}=0 and y_{fc}=0

Model	Solution				Proposed solution				Pressure acting on the footing		A_{min} (m^2)
	R (m)	y_0 (m)	α (Rad)	M_R (kN-m)	R (m)	y_0 (m)	α (Rad)	M_R (kN-m)	σ_{maxpaf} (kN/m^2)	σ_{minpaf} (kN/m^2)	
Example 1A: P_D=800 kN, P_L=700 kN, P=1500 kN, M_{yD}=200 kN-m, M_{yL}=100 kN-m, M_y=300 kN-m, M_{xD}=300 kN-m, M_{xL}=200 kN-m, M_x=500 kN-m											
NM	No solution										
LR	2.05	-	0.5404	583.10	2.05	-	0.5404	583.10	199.79	27.44	13.20
Example 1B: P_D=700 kN, P_L=600 kN, P=1300 kN, M_{yD}=200 kN-m, M_{yL}=100 kN-m, M_y=300 kN-m, M_{xD}=300 kN-m, M_{xL}=200 kN-m, M_x=500 kN-m											
NM	No solution										
LR	1.98	-	0.5404	583.10	2.00	-	0.5404	583.10	196.25	10.65	12.57
Example 1C: P_D=600 kN, P_L=500 kN, P=1100 kN, M_{yD}=200 kN-m, M_{yL}=100 kN-m, M_y=300 kN-m, M_{xD}=300 kN-m, M_{xL}=200 kN-m, M_x=500 kN-m											
NM	1.91	-1.55	0.5404	583.10	1.95	-1.61	0.5404	583.10	190.73	0	11.95
LR	2.12	-	0.5404	583.10	2.125	-	0.5404	583.10	154.91	0.17	14.19
Example 1D: P_D=500 kN, P_L=400 kN, P=900 kN, M_{yD}=200 kN-m, M_{yL}=100 kN-m, M_y=300 kN-m, M_{xD}=300 kN-m, M_{xL}=200 kN-m, M_x=500 kN-m											
NM	1.87	-1.15	0.5404	583.10	1.95	1.61	0.5404	583.10	190.73	0	11.95
LR	2.59	-	0.5404	583.10	2.60	-	0.5404	583.10	84.62	0.14	21.24

where: σ_{maxpaf} is the maximum pressure acting on the footing, σ_{minpaf} is the minimum pressure acting on the footing.

Table 5 Minimum cost design of Example 1 of the MPLR against the NM: x_{fc}=0 and y_{fc}=0

Model	Proposed solution					A_{sx} (cm^2)	A_{sy} (cm^2)	s_x (cm)	s_y (cm)	d (cm)	ρ_x	ρ_y	C_{min} (USD)
	R (m)	y_0 (m)	α (Rad)	M_{Ru} (kN-m)	σ_u (kN/m^2)								
Example 1A: P_D=800 kN, P_L=700 kN, P_u=2080 kN, M_{yD}=200 kN-m, M_{yL}=100 kN-m, M_{yu}=400 kN-m, M_{xD}=300 kN-m, M_{xL}=300 kN-m, M_{xu}= 680 kN-m													
NM	No solution												
LR	2.05	-	0.5317	788.92	274.14	64.39	64.39	32.05	32.05	47.50	0.00333	0.00333	10.85C_c
Example 1B: P_D=700 kN, P_L=600 kN, P_u=1800 kN, M_{yD}=200 kN-m, M_{yL}=100 kN-m, M_{yu}=400 kN-m, M_{xD}=300 kN-m, M_{xL}=200 kN-m, M_{xu}=680 kN-m													
NM	No solution												
LR	2.00	-	0.5317	788.92	268.80	56.19	63.55	35.82	31.67	42.50	0.00333	0.00377	9.73C_c
Example 1C: P_D=600 kN, P_L=500 kN, P_u=1520 kN, M_{yD}=200 kN-m, M_{yL}=100 kN-m, M_{yu}=400 kN-m, M_{xD}=300 kN-m, M_{xL}=200 kN-m, M_{xu}=680 kN-m													
NM	1.95	-1.65	0.5317	788.92	260.42	48.38	52.24	40.56	37.56	37.50	0.00333	0.00360	8.15C_c
LR	2.125	-	0.5317	788.92	211.83	59.72	63.89	35.82	33.49	42.50	0.00333	0.00356	10.79C_c
Example 1D: P_D=500 kN, P_L=400 kN, P_u=1240 kN, M_{yD}=200 kN-m, M_{yL}=100 kN-m, M_{yu}=400 kN-m, M_{xD}=300 kN-m, M_{xL}=200 kN-m, M_{xu}=680 kN-m													
NM	1.95	-1.31	0.5317	788.92	241.53	43.62	54.17	44.98	36.22	32.50	0.00347	0.00431	7.28C_c
LR	2.60	-	0.5317	788.92	115.54	64.74	64.69	40.57	40.60	37.50	0.00333	0.00333	14.12C_c

Table 6 Minimum area of Example 2 of the MPLR against the NM: $x_{fc}=R/2$ and $y_{fc}=0$

Model	Solution				Proposed solution				Pressure acting on the footing		A_{min} (m^2)
	R (m)	y_0 (m)	α (Rad)	M_R (kN-m)	R (m)	y_0 (m)	α (Rad)	M_R (kN-m)	σ_{maxpaf} (kN/m^2)	σ_{minpaf} (kN/m^2)	
Example 2A: P_D=800 kN, P_L=600 kN, P=1400 kN, M_{yD}=-500 kN-m, M_{yL}=-500 kN-m, M_y=-1000 kN-m, M_{xD}=300 kN-m, M_{xL}=200 kN-m, M_x=500 kN-m											
NM	No solution										
LR	2.07	-	-	672.01	2.10	-	-	686.22	195.40	6.71	13.85
Example 2B: P_D=700 kN, P_L=500 kN, P=1200 kN, M_{yD}=-500 kN-m, M_{yL}=-500 kN-m, M_y=-1000 kN-m, M_{xD}=300 kN-m, M_{xL}=200 kN-m, M_x=500 kN-m											
NM	1.92	-1.88	0.2994	522.59	1.95	-1.91	0.3277	528.11	194.03	0	11.95
LR	1.91	-	-	520.88	2.00	-	-	538.52	181.20	9.79	12.57
Example 2C: P_D=600 kN, P_L=400 kN, P=1000 kN, M_{yD}=-500 kN-m, M_{yL}=-500 kN-m, M_y=-1000 kN-m, M_{xD}=300 kN-m, M_{xL}=200 kN-m, M_x=500 kN-m											
NM	1.84	-1.56	-0.1593	506.36	1.85	-1.58	-0.1489	505.59	196.97	0	10.75
LR	2.00	-	-	500.00	2.00	-	-	500.00	159.15	0	12.57
Example 2D: P_D=500 kN, P_L=300 kN, P=800 kN, M_{yD}=-500 kN-m, M_{yL}=-500 kN-m, M_y=-1000 kN-m, M_{xD}=300 kN-m, M_{xL}=200 kN-m, M_x=500 kN-m											
NM	1.84	-0.96	-0.4862	565.42	1.85	-0.98	-0.4795	563.56	196.13	0	10.75
LR	2.50	-	-	500.00	2.50	-	-	500.00	81.49	0	19.63

does not present a solution for the two first examples, and for the last two examples the NM governs.

Table 6 of the example 2 ($x_{fc}=R/2$ and $y_{fc}=0$) for minimum area of the MPLR show the following: the smallest values for R and A_{min} are presented in the MPLR because the NM does not present a solution for the first example, and for the last three examples the NM governs.

Table 7 of the example 2 ($x_{fc}=R/2$ and $y_{fc}=0$) for minimum cost design of the MPLR show the following: the smallest values for A_{sx}, A_{sy}, d and C_{min} are presented in the MPLR because the NM does not present a solution for the first example, and for the last three examples the NM governs for A_{sx} (except in examples 2B and 2C), A_{sy}, d (except in example 2D) and C_{min}.

Fig. 9 shows the minimum cost of examples 1, 2, 3 for the four cases.

Fig. 9 shows the following for the three examples: The lowest cost appears in case 1 for all examples, because the factored soil pressure acting on the footing is greater. The largest cost appears in case 4 for all examples, because the factored soil pressure acting on the footing is lower.

Fig. 10 presents the results of Example 1 of the MPLR against the NM. Fig. 10(a) shows the minimum area and Fig. 10(b) presents the minimum cost.

Fig. 10(a) presents the following results (Example 1): The smaller area appears in the NM compared to the MPLR in Examples 1C and 1D, and the smaller area appears in the MPLR compared to the NM in Examples 1A and 1B since the NM has no solution. The largest difference appears in example 1D of 1.78 times the MPLR than the NM.

Fig. 10(b) shows the following results (Example 1): The smaller cost appears in the NM compared to the MPLR in Examples 1C and 1D, and the smaller cost appears in the MPLR compared to the NM in Examples 1A and 1B since the NM has no solution. The largest difference appears in example 1D of 1.94 times the MPLR than the NM.

Table 7 Minimum cost design of Example 2 of the MPLR against the NM: $x_{fc}=R/2$ and $y_{fc}=0$

Model	Proposed solution					A_{sx} (cm^2)	A_{sy} (cm^2)	s_x (cm)	s_y (cm)	d (cm)	ρ_x	ρ_y	C_{min} (USD)
	R (m)	y_0 (m)	α (Rad)	M_{Ru} (kN-m)	σ_u (kN/m^2)								
Example 2A: P_D=800 kN, P_L=600 kN, P_u=1920 kN, M_{yD}=-500 kN-m, M_{yL}=-500 kN-m, M_{yu}=-1400 kN-m, M_{xD}=300 kN-m, M_{xL}=200 kN-m, M_{xu}=680 kN-m													
NM	No solution												
LR	2.10	-	0.7361	917.53	264.73	86.79	86.79	24.36	24.36	62.50	0.00333	0.00333	15.12C_c
Example 2B: P_D=700 kN, P_L=500 kN, P_u=1640 kN, M_{yD}=-500 kN-m, M_{yL}=-500 kN-m, M_{yu}=-1400 kN-m, M_{xD}=300 kN-m, M_{xL}=200 kN-m, M_{xu}=680 kN-m													
NM	1.95	-1.94	0.2847	708.52	263.80	73.52	61.22	26.69	32.05	47.50	0.00400	0.00333	10.26C_c
LR	2.00	-	0.3393	721.11	216.64	71.35	69.41	28.21	29.00	52.50	0.00342	0.00333	11.60C_c
Example 2C: P_D=600 kN, P_L=400 kN, P_u=1360 kN, M_{yD}=-500 kN-m, M_{yL}=-500 kN-m, M_{yu}=-1400 kN-m, M_{xD}=300 kN-m, M_{xL}=200 kN-m, M_{xu}=680 kN-m													
NM	1.85	-1.56	-0.2059	694.67	269.17	94.13	45.91	19.77	40.53	37.50	0.00684	0.00333	8.59C_c
LR	2.00	-	-0.0588	681.18	216.64	82.63	56.19	24.36	35.82	42.50	0.00490	0.00333	10.33C_c
Example 2D: P_D=500 kN, P_L=300 kN, P_u=1080 kN, M_{yD}=-500 kN-m, M_{yL}=-500 kN-m, M_{yu}=-1400 kN-m, M_{xD}=300 kN-m, M_{xL}=200 kN-m, M_{xu}=680 kN-m													
NM	1.85	-0.90	-0.5328	789.43	273.27	78.06	58.05	23.84	32.05	47.50	0.00448	0.00333	9.63C_c
LR	2.50	-	-0.0734	681.84	110.56	97.48	62.07	25.85	40.60	37.50	0.00523	0.00333	14.12C_c

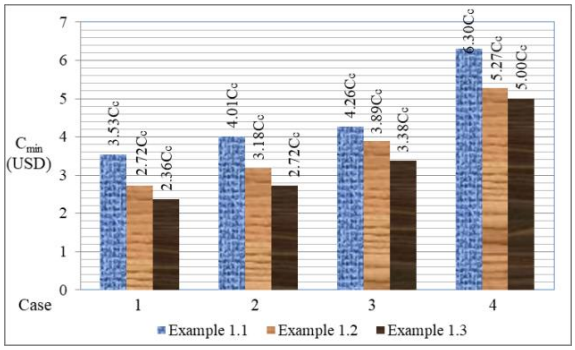

(a) Example 1

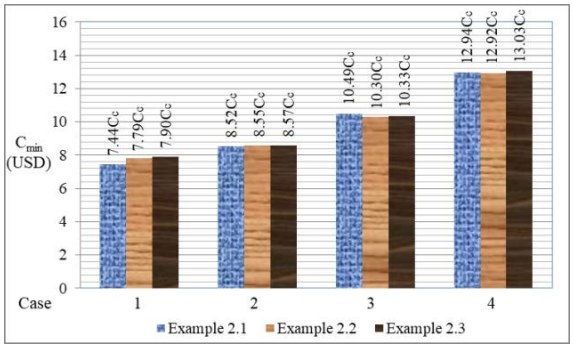

(b) Example 2

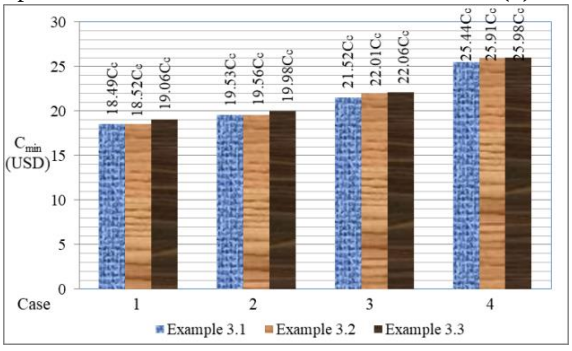

(c) Example 3

Fig. 9 Minimum cost of the three examples for the four cases

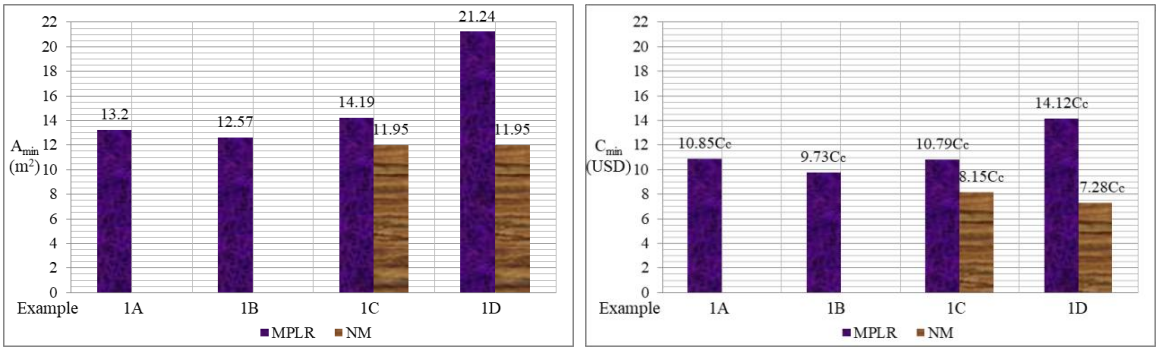

(a) Minimum area (b) Minimum cost

Fig. 10 Comparison of Example 1 of MPLR against the NM

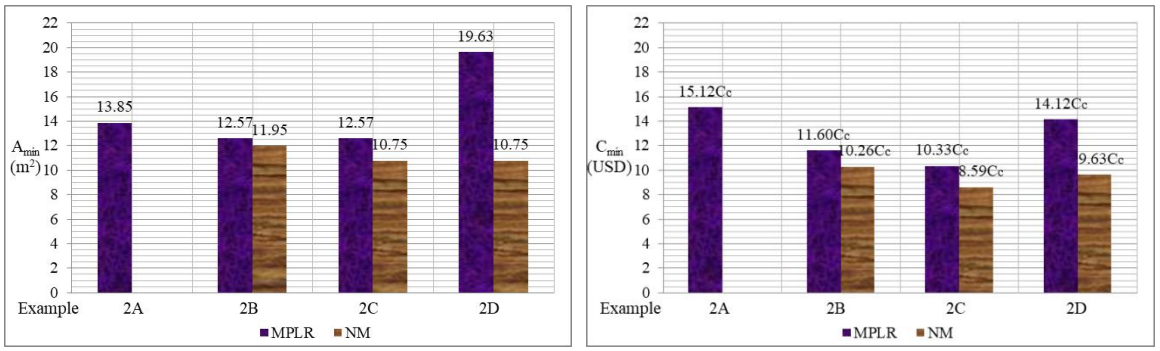

(a) Minimum area (b) Minimum cost

Fig. 11 Comparison of Example 2 of MPLR and NM

Fig. 11 presents the results of Example 2 of the MPLR against the NM. Fig. 11(a) shows the minimum area and Fig. 11(b) presents the minimum cost.

Fig. 11(a) presents the following results (Example 2): The smaller area appears in the NM compared to the MPLR in Examples 1B, 1C and 1D, and the smaller area appears in the MPLR compared to the NM in Example 1A since the NM has no solution. The largest difference appears in example 1D of 1.83 times the MPLR than the NM.

Fig. 11(b) shows the following results (Example 2): The smaller cost appears in the NM compared to the MPLR in Examples 1B, 1C and 1D, and the smaller cost appears in the MPLR compared to the NM in Example 1A since the NM has no solution. The largest difference appears in example 1D of 1.47 times the MPLR than the NM.

5. Conclusions

This paper shows a model to estimate the minimum cost design (thickness and areas of reinforcing steel in both directions) in a circular isolated footing with an eccentric column considering that the area in contact with the ground works partially in compression, that is, a part of the contact surface of the footing works in compression and the other part has zero pressure.

This research shows the minimum cost design for a circular isolated footing under biaxial bending. Assuming that the footing is rigid and supported on elastic soils, the column is eccentrically positioned and the pressure diagram is linear.

The model Luévanos-Rojas *et al*. (2024b) is shown below: the independent variables (known data) are R, c_1, c_2, x_{fc}, y_{fc}, P_u, M_{xu} and M_{yu}, and the dependent variables are C_{min}, A_{sx}, A_{sy}, s_x, s_y, d, ρ_x and ρ_y (data to estimate).

The new model is shown as follows: the independent variables (known data) are σ_u, c_1, c_2, x_{fc}, y_{fc}, R, c_1, c_2, x_{fc}, y_{fc}, α, y_0, P_u, M_{xu} and M_{yu}, and the dependent variables are C_{min}, A_{sx}, A_{sy}, s_x, s_y, d, ρ_x and ρ_y (data to estimate).

The contributions of this paper are:

1) Some engineers obtain the thickness and areas of reinforcing steel of a circular isolated footing under biaxial bending, but considering a uniform pressure with a concentric column.

2) Another engineering practice to estimate the thickness and areas of reinforcing steel using optimization techniques, but the column is in the center of the base and the contact area of the footing operates completely in compression (Lopez-Chavarria *et al*. 2019).

3) Other engineers determine the thickness and areas of reinforcing steel of a circular isolated footing under biaxial bending with an eccentric column supported on elastic soils, but the area works completely in compression (Luévanos-Rojas *et al*. 2024b).

4) The new model can be adapted to other construction codes, considering the resistant moments, the bending shears that the concrete can resist and the punching shear that the concrete can resist, according to each code.

5) This model presents a great saving for minimum area compared with the model Luévanos-Rojas *et al*. (2024b) of 15.79% in Example 1C and 43.74% in Example 1D (see Table 4), 4.93% in Example 2B, 14.48% in Example 2C and 45.24% in Example 2D (see Table 6).

6) The new model presents a great saving for minimum cost design compared with the model Luévanos-Rojas *et al*. (2024b) of 24.47% in Example 1C and 48.44% in Example 1D (see Table 5), 11.55% in Example 2B, 16.84% in Example 2C and 31.80% in Example 2D (see Table 7).

Suggestions for the following investigations may be:

1.- Minimum surface for a rectangular isolated footing with an eccentric column considering that the area in contact with the ground works partially in compression.

2.- Minimum cost design for a rectangular isolated footing with an eccentric column considering that the area in contact with the ground works partially in compression.

Acknowledgements

The research described in this paper was financially supported by the Universidad Autónoma de Coahuila and Universidad Juárez del Estado de Durango, Mexico.

References

ACI 318S-14 (American Concrete Institute) (2014), Building Code Requirements for Structural Concrete and Commentary, Committee 318.

Agrawal, R. and Hora, M.S. (2012), "Nonlinear interaction behaviour of infilled frame-isolated footings-soil system subjected to seismic loading", *Struct. Eng. Mech.*, **44**(1), 85-107.

https://doi.org/10.12989/sem.2012.44.1.085.
Aguilera-Mancilla, G., Luévanos-Rojas, A., López-Chavarría, S. and Medina-Elizondo, M. (2019), "Modeling for the strap combined footings Part I: Optimal dimensioning", *Steel Compos. Struct.*, **30**(2), 97-108. https://doi.org/10.12989/scs.2019.30.2.097.
Al-Ansari, M.S. (2013), "Structural cost of optimized reinforced concrete isolated footing", *Int. Scholar. Sci. Res. Innov.*, **7**(4), 193-200.
Al-Ansari, M.S. (2014), "Cost of reinforced concrete paraboloid shell footing", *J. Struct. Anal. Des.*, **1**(3), 111-119.
Alazwari, M.A., Daikh, A.A., Houari, M.S.A., Tounsi, A. and Eltaher, M.A. (2021), "On static buckling of multilayered carbon nanotubes reinforced composite nanobeams supported on non-linear elastic foundations", *Steel Compos. Struct.*, **40**(3), 389-404. https://doi.org/10.12989/scs.2021.40.3.389.
Alijani, M. and Bidgoli, M.R. (2018), "Agglomerated SiO2 nanoparticles reinforced-concrete foundations based on higher order shear deformation theory: Vibration analysis", *Adv. Concrete Constr.*, **6**(6), 585-610. https://doi.org/10.12989/acc.2018.6.6.585.
Anil, Ö., Akbaş, S.O., BabagĪray, S., Gel, A.C. and Durucan, C. (2017), "Experimental and finite element analyses of footings of varying shapes on sand", *Geomech. Eng.*, **12**(2), 223-238. https://doi.org/10.12989/gae.2017.12.2.223.
Basudhar, P.K., Dey, A. and Mondal, A.S. (2012), "Optimal cost-analysis and design of circular footings", *Int. J. Eng. Technol. Innov.*, **2**(4), 243-264.
Dagdeviren, U. (2016), "Shear stresses below the rectangular foundations subjected to biaxial bending", *Geomech. Eng.*, **10**(2), 189-205. https://doi.org/10.12989/gae.2016.10.2.189.
Garay-Gallegos, J.R., Luévanos-Rojas, A., López-Chavarría, S., Medina-Elizondo, M., Aguilera-Mancilla, G. and García-Canales, E. (2022), "A comparative study between the new model and the current model for T-shaped combined footings", *Geomech. Eng.*, **30**(6), 525-538. https://doi.org/10.12989/gae.2022.30.6.525.
García-Galván, M., Luévanos-Rojas, A., López-Chavarría, S., Medina-Elizondo, M. and Rivera-Mendoza, J.B. (2022), "A general model for rectangular footings. Part I: optimal Surface", *DYNA: revista de la Facultad de Minas. Universidad Nacional de Colombia. Sede Medellín*, **89**(221), 132-141. https://doi.org/10.15446/dyna.v89n221.100028.
García-Galván, M., Luévanos-Rojas, A., López-Chavarría, S., Medina-Elizondo, M. and Rivera-Mendoza, J.B. (2022), "A comparative study between trapezoidal combined footings and T-shaped combined footings", *Couple. Syst. Mech.*, **11**(3), 233-257. https://doi.org/10.12989/csm.2022.11.3.233.
Garcia-Graciano, M.L., Luévanos-Rojas, A., López-Chavarría, S. and Medina-Elizondo, M. (2022), "Mathematical modeling for corner strap combined footings resting on the ground: Part 1", *Computación y Sistemas*, **26**(4), 1429-1443. http://doi.org/10.13053/cys-26-4-4080.
Golewski, G.L. (2019), "New principles for implementation and operation of foundations for machines: A review of recent advances", *Struct. Eng. Mech.*, **71**(3), 317-327. https://doi.org/10.12989/sem.2019.71.3.317.
Gör, M. (2022), "Analyzing the bearing capacity of shallow foundations on two-layered soil using two novel cosmology-based optimization techniques", *Smart Struct. Syst.*, **29**(3), 513-522. https://doi.org/10.12989/sss.2022.29.3.513.
Hadzalic, E., Ibrahimbegovic, A. and Dolarevic, S. (2018), "Failure mechanisms in coupled soil-foundation systems", *Couple. Syst. Mech.*, **7**(1), 27-42. https://doi.org/10.12989/csm.2018.7.1.027.
Hadzalic, E., Ibrahimbegovic, A. and Dolarevic, S. (2018), "Failure mechanisms in coupled poro-plastic medium", *Couple. Syst. Mech.*, **7**(1), 43-59. https://doi.org/10.12989/csm.2018.7.1.043.
Hadzalic, E., Ibrahimbegovic, A. and Dolarevic, S. (2018), "Fluid-structure interaction system predicting both internal pore pressure and outside hydrodynamic pressure", *Couple. Syst. Mech.*, **7**(6), 649-668. https://doi.org/10.12989/csm.2018.7.6.649.
Hadzalic, E., Ibrahimbegovic, A. and Dolarevic, S. (2020), "3D thermo-hydro-mechanical coupled discrete beam lattice model of saturated poro-plastic medium", *Couple. Syst. Mech.*, **9**(2), 125-145. https://doi.org/10.12989/csm.2020.9.2.125.

Himeur, N., Mamen, B., Benguediab, S., Bouhadra, A., Menasria, A., Bouchouicha, B., Bourada, F., Benguediab, M. and Tounsi, A. (2022), "Coupled effect of variable Winkler–Pasternak foundations on bending behavior of FG plates exposed to several types of loading", *Steel Compos. Struct.*, **44**(3), 353-369. https://doi.org/10.12989/scs.2022.44.3.353.

Ibrahimbegovic, A. and Mejia-Nava, R.A. (2021), "Heterogeneities and material-scales providing physically based damping to replace Rayleigh damping for any structure size", *Couple. Syst. Mech.*, **10**(3), 201-216. https://doi.org/10.12989/csm.2021.10.3.201.

Jelusic, P. and Zlender, B. (2018), "Optimal design of pad footing based on MINLP optimization", *Soil. Found.*, **58**(2), 277-289. https://doi.org/10.1016/j.sandf.2018.02.002.

Kaur, A. and Kumar, A. (2016), "Behavior of eccentrically inclined loaded footing resting on fiber reinforced soil", *Geomech. Eng.*, **10**(2), 155-174. https://doi.org/10.12989/gae.2016.10.2.155.

Khajehzadeh, M., Taha, M.R. and Eslami, M. (2014), "Multi-objective optimization of foundation using global-local gravitational search algorithm", *Struct. Eng. Mech.*, **50**(3), 257-273. http://doi.org/10.12989/sem.2014.50.3.257.

Kim-Sánchez, D.S., Luévanos-Rojas, A., Barquero-Cabrero, J.D., López-Chavarría, S., Medina-Elizondo, M. and Luévanos-Soto, I. (2022), "A new model for the complete design of circular isolated footings considering that the contact surface works partially under compression", *Int. J. Innov. Comput. I.*, **18**(6), 1769-1784.

Lee, J., Jeong, S. and Lee, J.K. (2015), "3D analytical method for mat foundations considering coupled soil springs", *Geomech. Eng.*, **8**(6), 845-850. https://doi.org/10.12989/gae.2015.8.6.845.

Lezgy-Nazargah, M., Mamazizi, A. and Khosravi, H. (2022), "Analysis of shallow footings rested on tensionless foundations using a mixed finite element model", *Struct. Eng. Mech.*, **81**(3), 379-394. https://doi.org/10.12989/sem.2022.81.3.379.

López-Chavarría, S., Luévanos-Rojas, A. and Medina-Elizondo, M. (2017a), "Optimal dimensioning for the corner combined footings", *Adv. Comput. Des.*, **2**(2), 169-183. https://doi.org/10.12989/acd.2017.2.2.169.

López-Chavarría, S., Luévanos-Rojas, A. and Medina-Elizondo, M. (2017b), "A mathematical model for dimensioning of square isolated footings using optimization techniques: general case", *Int. J. Innov. Comput. I.*, **13**(1), 67-74.

López-Chavarría, S., Luévanos-Rojas, A. and Medina-Elizondo, M. (2017c), "A new mathematical model for design of square isolated footings for general case", *Int. J. Innov. Comput. I.*, **13**(4), 1149-1168.

López-Chavarría, S., Luévanos-Rojas, A., Medina-Elizondo, M., Sandoval-Rivas, R. and Velázquez-Santillán, F. (2019), "Optimal design for the reinforced concrete circular isolated footings", *Adv. Comput. Des.*, **4**(3), 273-294. https://doi.org/10.12989/acd.2019.4.3.273.

Luat, N.V., Lee, K. and Thai, D.K. (2020), "Application of artificial neural networks in settlement prediction of shallow foundations on sandy soils", *Geomech. Eng.*, **20**(5), 385-397. https://doi.org/10.12989/gae.2020.20.5.385.

Luévanos-Rojas, A. (2014a), "A comparative study for dimensioning of footings with respect to the contact surface on soil", *Int. J. Innov. Comput. I.*, **10**(4), 1313-1326.

Luévanos-Rojas, A. (2014b), "Design of isolated footings of circular form using a new model", *Struct. Eng. Mech.*, **52**(4), 767-786. https://doi.org/10.12989/sem.2014.52.4.767.

Luévanos-Rojas, A. (2014c), "Design of boundary combined footings of rectangular shape using a new model", *Dyna*, **81**(188), 199-208. https://doi.org/10.15446/dyna.v81n188.41800.

Luévanos-Rojas, A. (2015a), "A new mathematical model for dimensioning of the boundary trapezoidal combined footings", *Int. J. Innov. Comput. I.*, **11**(4), 1269-1279.

Luévanos-Rojas, A. (2015b), "Design of boundary combined footings of trapezoidal form using a new model", *Struct. Eng. Mech.*, **56**(5), 745-765. http://doi.org/10.12989/sem.2015.56.5.745.

Luévanos-Rojas, A. (2016a), "A comparative study for the design of rectangular and circular isolated footings using new models", *Dyna*, **83**(196), 149-158. https://doi.org/10.15446/dyna.v83n196.51056.

Luévanos-Rojas, A. (2016b), "A mathematical model for the dimensioning of combined footings of rectangular shape", *Revista Técnica de la Facultad de Ingeniería Universidad del Zulia*, **39**(1), 3-9.

Luévanos-Rojas, A. (2016c), "A new model for the design of rectangular combined boundary footings with

two restricted opposite sides", *Revista ALCONPAT*, **6**(2), 172-187. https://doi.org/10.21041/ra.v6i2.137.

Luévanos-Rojas, A. (2023a), "Minimum cost design for rectangular isolated footings taking into account that the column is located in any part of the footing", *Build.*, **13**(9), 1-16. https://doi.org/10.3390/buildings13092269.

Luévanos-Rojas, A. (2023b), "Optimization for trapezoidal combined footings: Optimal design", *Adv. Concrete Constr.*, **16**(1), 21-34. https://doi.org/10.12989/acc.2023.16.1.021.

Luévanos-Rojas, A. (2023c), "New model for complete design of rectangular isolated footings taking into account that the contact surface works partially in compression", *Revista ALCONPAT*, **13**(2), 192-219. https://doi.org/10.21041/ra.v13i2.671.

Luévanos-Rojas, A., Barquero-Cabrero, J.D., López-Chavarría, S. and Medina-Elizondo, M. (2017b), "A comparative study for design of boundary combined footings of trapezoidal and rectangular forms using new models", *Couple. Syst. Mech.*, **6**(4), 417-437. https://doi.org/10.12989/csm.2017.6.4.417.

Luévanos-Rojas, A., Barquero-Cabrero, J.D., López-Chavarría, S., Medina-Elizondo, M., Vela-Moreno, V.B. and Barraza-Saucedo, R. (2022), "Costo mínimo para zapatas combinadas trapezoidales de concreto reforzado apoyadas sobre el terreno", *Revista Internacional de Investigación e Innovación Tecnológica*, **10**(56), 62-85.

Luévanos-Rojas, A., Faudoa-Herrera, J.G. andrade-Vallejo, R.A. and Cano-Alvarez, M.A. (2013), "Design of isolated footings of rectangular form using a new model", *Int. J. Innov. Comput. I.*, **9**(10), 4001-4022.

Luévanos-Rojas, A., López-Chavarría, S. and Medina-Elizondo, M. (2017a), "Optimal design for rectangular isolated footings using the real soil pressure", *Ing. Invest.*, **37**(2), 25-33. https://doi.org/10.15446/ing.investig.v37n2.61447.

Luévanos-Rojas, A., López-Chavarría, S. and Medina-Elizondo, M. (2018a), "A new model for T-shaped combined footings Part I: Optimal dimensioning", *Geomech. Eng.*, **14**(1), 51-60. https://doi.org/10.12989/gae.2018.14.1.051.

Luévanos-Rojas, A., López-Chavarría, S. and Medina-Elizondo, M. (2018b), "A new model for T-shaped combined footings Part II: Mathematical model for design", *Geomech. Eng.*, **14**(1), 61-69. https://doi.org/10.12989/gae.2018.14.1.061.

Luévanos-Rojas, A., López-Chavarría, S., Medina-Elizondo, M., Sandoval-Rivas, R. and Farías-Montemayor, O.M. (2020), "An analytical model for the design of corner combined footings", *Revista ALCONPAT*, **10**(3), 317-335. https://doi.org/10.21041/ra.v10i3.432.

Luévanos-Rojas, A., Moreno-Landeros, V.M., Santiago-Hurtado, G., Olguin-Coca, F.J., López-León, L.D., Baltazar-Zamora, M.A. and Diaz-Gurrola, E.R. (2024b), "Mathematical modeling of the optimal cost for the design of circular isolated footings with eccentric column", *Math.*, **12**(5), 1-19. https://doi.org/10.3390/math12050733.

Luévanos-Rojas, A., Santiago-Hurtado, G., Moreno-Landeros, V.M., Olguin-Coca, F.J., López-León, L.D. and Diaz-Gurrola, E.R. (2024a), "Mathematical modeling of the optimal cost for the design of strap combined footings", *Math.*, **12**(2), 1-20. https://doi.org/10.3390/math12020294.

Luévanos-Soto, I., Luévanos-Rojas, A., Moreno-Landeros, V.M. and Santiago-Hurtado, G. (2024), "Minimum area for circular isolated footings with eccentric column taking into account that the surface in contact with the ground works partially in compression", *Couple. Syst. Mech.*, **13**(3), 201-217. https://doi.org/10.12989/csm.2024.13.3.201.

Malapur, M.M., Cholappanavar, P. and Fernandes, R.J. (2018), "Optimization of RC column and footings using genetic algorithm", *Int. Res. J. Eng. Technol. (IRJET)*, **5**(8), 546-552.

Mohebkhah, A. (2017), "Bearing capacity of stripfootingson a stone masonry trench in clay", *Geomech. Eng.*, **13**(2), 255-267. https://doi.org/10.12989/gae.2017.13.2.255.

Montes-Paramo, P., Luévanos-Rojas, A., López-Chavarría, S., Medina-Elizondo, M. and Sandoval-Rivas, R. (2023), "Optimal area for rectangular combined footings assuming that the contact surface with the soil works partially to compression", *Ingeniería Investigación y Tecnología*, **24**(02), 1-15. https://doi.org/10.22201/fi.25940732e.2023.24.2.012.

Moreno-Hernández, M.A., Luévanos-Rojas, A., López-Chavarría, S. and Medina-Elizondo, M. (2022), "Mathematical modeling for corner strap combined footings resting on the ground: Part 1", *Computación*

y Sistemas, **26**(3), 1259-1272. http://doi.org/10.13053/cys-26-3-4079.

Pasillas-Orona, A.I., Luévanos-Rojas, A., López-Chavarría, S., Medina-Elizondo, M. and Aguilera-Mancilla, G. (2020), "Un modelo optimizado para zapatas combinadas trapezoidales apoyadas sobre el terreno: Superficie óptima", *Acta Universitaria*, **30**, 1-18. http://doi.org/10.15174/au.2020.2973.

Rad, A.B. (2012), "Static response of 2-D functionally graded circular plate with gradient thickness and elastic foundations to compound loads", *Struct. Eng. Mech.*, **44**(2), 139-161. https://doi.org/10.12989/sem.2012.44.2.139.

Ramu, K. and Madhav, M.R. (2010), "Response of rigid footing on reinforced granular fill over soft soil", *Geomech. Eng.*, **2**(4), 281-302. https://doi.org/10.12989/gae.2010.2.4.281.

Rawat, S. and Mittal, R.K. (2018), "Optimization of eccentrically loaded reinforced-concrete isolated footings", *Pract. Period. Struct. Des. Constr.*, **23**(2), 06018002. https://doi.org/10.1061/(ASCE)SC.1943-5576.0000366.

Rivera-Mendoza, J.B., Luévanos-Rojas, A., López-Chavarría, S., Medina-Elizondo, M. and García-Galván, M. (2022), "General model for rectangular footings part II: modeling for design", *Dyna*, **89**(223), 9-18. https://doi.org/10.15446/dyna.v89n223.100030.

Rizwan, M., Alam, B., Rehman, F.U., Masud, N., Shahzada, K., Masud, T. (2012), "Cost optimization of combined footings using modified complex method of box", *Int. J. Adv. Struct. Geotech. Eng.*, **1**(1), 24-28.

Soto-Garcia, S., Luévanos-Rojas, A., Barquero-Cabrero, J.D., López-Chavarría, S., Medina-Elizondo, M., Farias-Montemayor, O.M. and Martinez-Aguilar, C. (2022), "A new model for the contact surface with soil of circular isolated footings considering that the contact surface works partially under compression", *Int. J. Innov. Comput. I.*, **18**(4), 1103-1116.

Turedi, Y., Emirler, B., Ornek, M. and Yildiz, A. (2019), "Determination of the bearing capacity of model ring footings: Experimental and numerical investigations", *Geomech. Eng.*, **18**(1), 29-39. https://doi.org/10.12989/gae.2019.18.1.029.

Vela-Moreno, V.B., Luévanos-Rojas, A., López-Chavarría, S., Medina-Elizondo, M., Sandoval-Rivas, R. and Martinez-Aguilar, C. (2022), "Optimal area for rectangular isolated footings considering that contact surface works partially to compression", *Struct. Eng. Mech.*, **84**(4), 561-573. https://doi.org/10.12989/sem.2022.84.4.561.

Velázquez-Santillán, F., Luévanos-Rojas, A., López-Chavarría, S., Medina-Elizondo, M. and Sandoval-Rivas, R. (2018), "Numerical experimentation for the optimal design for reinforced concrete rectangular combined footings", *Adv. Comput. Des.*, **3**(1), 49-69. https://doi.org/10.12989/acd.2018.3.1.049.

Yáñez-Palafox, J.A., Luévanos-Rojas, A., López-Chavarría, S. and Medina-Elizondo, M. (2019), "Modeling for the strap combined footings Part II: Mathematical model for design", *Steel Compos. Struct.*, **30**(2), 109-121. https://doi.org/10.12989/scs.2019.30.2.109.

AI